Modeling the Thermal Response of Porcine Cartilage to Laser Irradiation

Sergio H. Díaz, Guillermo Aguilar, Enrique J. Lavernia, and Brian J. F. Wong

***Abstract*—During laser irradiation of biological tissue, a number of physical processes take place that determine temperature elevation and thermal damage rates. Some of those important to laser–tissue interaction are: 1) propagation of light in scattering media; 2) transformation of laser light into photochemical, acoustic, or thermal energy; 3) tissue–tissue and tissue–environment heat and mass transfer; 4) and the occurrence of low-energy phase transformations responsible for structural alterations. The aim of this study was to formulate a finite-element model (FEM) able to predict the temperature distribution in a slab of porcine nasal cartilage during laser irradiation. The FEM incorporates heat diffusion, light propagation in tissue, and water evaporation from the surfaces of the slab. Numerical results were compared to experimental temperature distributions where surface and internal temperatures were measured while heating cartilage using a pulsed Nd : YAG laser ($\lambda = 1.32$ μm). Rectangular specimens, 1–4-mm thick, were secured perpendicular to the laser beam and irradiated for 1–15 s using different laser-beam powers (1–10 W).**

***Index Terms*—Cartilage reshaping, finite element modeling, laser-beam profile, Monte Carlo, plastic surgery, stress relaxation, tissue damage.**

I. Introduction

LASER-ASSISTED reshaping of cartilage is a new surgical procedure designed to allow *in situ* treatment of deformities in the head and neck with less morbidity than traditional approaches [1]. During laser irradiation, mechanically deformed cartilage undergoes accelerated stress relaxation that permits tissue to be reshaped into new stable configurations. Clinically, reshaped cartilage can then be used to reconstruct the framework of structures within the head and neck, such as the ear, nose, larynx, and trachea. Since laser-assisted reshaping of cartilage (LARC) can be performed using minimally invasive techniques with less morbidity than traditional reconstructive procedures, it has the potential to alter radically the practice of aesthetic and reconstructive cranio-maxillo-facial surgery. The principal advantage of using laser radiation to generate thermal energy in tissue is the precise control of the space–time dependent temperature distribution.

Optimization of the reshaping process requires characterization of the temperature-dependent stress relaxation and correlation of these changes with observed alterations in cartilage physical properties (e.g., elastic modulus, thermal diffusivity, and optical scattering). While animal and human studies have demonstrated clinical feasibility [2], [3], the fundamental biophysical mechanisms accompanying laser reshaping are largely unknown. It has been suggested that the mechanism responsible of laser reshaping is primarily associated with a phase transformation of cartilaginous bound water to free water taking place at a temperature of $T_w \cong 65$ °C [4]. On the other hand, protein denaturation and subsequent cell death are time- and temperature-dependent processes, where damage is exponentially dependent on temperature and linearly dependent on time of exposure [5]. Cartilage specimen must be heated to the critical transition temperature for reshaping, while maintaining temperature and laser exposure to a minimum to reduce cellular injury.

The above-mentioned boundary conditions require accurate prediction of the temperature distribution during laser irradiation. The purpose of this study was then to develop a finite-element model (FEM) able to predict the temperature distribution in a slab of porcine nasal cartilage (PNC) during laser irradiation. The model incorporates heat diffusion, light propagation in tissue, and water evaporation from the surfaces of the slab. Numerical results are then compared to experimental characterization of the thermal distribution in PNC during sustained high power Nd : YAG laser ($\lambda = 1.32$ μm) irradiation, where surface and internal temperature of the specimen are measured using contact (thermocouple) and noncontact (infrared emission) probes.

II. The Heat Equation

The temperature response of tissue to laser irradiation is governed by the following:

$$\rho c \frac{\partial T}{\partial t} = \kappa \frac{\partial^2 T}{\partial z^2} + Q_i \tag{1}$$

where T is temperature (K), ρ is density (kg/m^3), c is the specific heat (J/kg·K) of the tissue, κ is the thermal conductivity (W/m·K), and Q_i is the rate of internal heating due to irradiation.

Transformation of light into thermal energy depends on the light fluence rate distribution $\phi(x, y, z)$ (W/m^2) and absorption coefficient μ_a (m^{-1}) of the tissue, such that

$$Q_i = \mu_a \phi(x, y, z). \tag{2}$$

Manuscript received June 4, 2001. This work was supported in part by the National Institutes of Health under Grant AR43419 and Grant DC 00170, in part by the Office of Naval Research under Grant N00014-94-0874, in part by the Department of Energy under Grant DE-FG03-91ER61227, and in part by the Air Force Office of Scientific Research.

S. H. Díaz and B. J. F. Wong are with the Beckman Laser Institute and Medical Clinic, University of California, Irvine, CA 92612 USA (e-mail: bjfwong@bli.uci.edu).

G. Aguilar is with the Beckman Laser Institute and Medical Clinic and the Center for Biomedical Engineering, University of California, Irvine, CA 92612 USA.

E. J. Lavernia is with the Department of Chemical and Biochemical Engineering and Material Science, University of California, Irvine, CA 92612 USA.

Publisher Item Identifier S 1077-260X(01)11235-9.

The $\phi(x, y, z)$ can be estimated as a function of penetration depth in tissue using various light distribution models [6]. In this work, $\phi(x, y, z)$ is estimated using a Monte Carlo algorithm developed by Wang *et al.* [7], [8]. The specimen thickness, tissue optical properties, and laser-beam power and diameter are used as input parameters to the code.

Water loss due to evaporation was also considered in the FEM. Evaporation occurs from the cartilage surface and the energy associated with the phase change is the latent heat of liquid vaporization. The energy required to sustain evaporation Q_{vap} must come from the internal energy of the liquid (free water in cartilage), which then must experience a reduction in temperature [9]. Water vaporization is a diffusion-limited surface loss phenomenon that depends primarily on surface characteristics such as local humidity and temperature-dependent mass diffusion coefficients [5]. Q_{vap} may be approximated as the product of evaporative mass flux and latent heat of vaporization [9]

$$Q_{\text{vap}} = n''_{\text{vap}} h_{fg} \tag{3}$$

where h_{fg} is the phase change enthalpy (J/kg). The mass flux n''_{vap} (kg/s m^2) of water vapor may be expressed as

$$n''_{\text{vap}} = h_m \left[\rho_{\text{vap, sat}}(T_s) - \rho_{\text{vap, }\infty}\right] \tag{4}$$

or as a mass-transfer rate n_{vap} (kg/s) given by

$$n_{\text{vap}} = h_m A_s \left[\rho_{\text{vap, sat}}(T_s) - \rho_{\text{vap, }\infty}\right] \tag{5}$$

where h_m is the convection mass-transfer coefficient (m/s), $\rho_{\text{vap,sat}}(T_s)$ is the density of saturated water vapor (kg/m^3) at the surface temperature (T_s) of the tissue (which can be obtained from thermodynamic tables of water), $\rho_{\text{vap},\infty}$ is the density of water vapor in air (kg/m^3) at room temperature, and A_s is the exposed surface area (m^2). The $\rho_{\text{vap},\infty}$ can be estimated from the relative humidity, Rh, as

$$Rh = \frac{P_v}{P_g} = \frac{\rho_{\text{vap, }\infty}}{\rho_{\text{vap, sat}}(T_\infty)} \tag{6}$$

where P_v is the partial pressure of vapor as it exists in the water vapor–air mixture and P_g the saturation vapor pressure at the same temperature.

III. Finite Element Model (FEM)

Problems involving time-dependent thermal and optical properties, irregular boundary conditions, or complex geometries are very often difficult to formulate using analytical solutions. Such problems can be solved by numerical methods, such as the finite difference method or the finite-element method. A numerical time-dependent solution of the heat equation has been obtained using a finite-element code (FEMBLAB, Comsol Inc., Burlington, MA) in order to calculate spatial and temporal temperature profiles $T(x, y, z, t)$ of irradiated tissue.

The FEM consists of approximately 1500 nodes and 6000 elements. Symmetry along YZ and XZ planes was used, as shown in Fig. 1. The following thermal properties of cartilage (measured or taken to be equal to those of water) were used in the numerical analysis: $\rho = 1.26$ kg/cm^3, $c = 4.0$ J/kg·K, $\kappa = 0.6$ W/m·K. The tissue initial temperature (T_o) varied between 18 °C–20 °C, room temperature (T_∞) ranged between 22 °C–23 °C. The thermal boundary condition at an air–tissue interface, top, bottom, and perimeter ($r_{\text{inf}} = 10$ mm) surfaces, accounted for convective heat loss (free convection) and water vaporization. The applied laser powers ranged from 1–10 W and irradiation times varied between 1–15 s. Laser spot radius (r_o) was 2.5 mm. Typical values of specimen thickness (D) ranged between 1–4 mm.

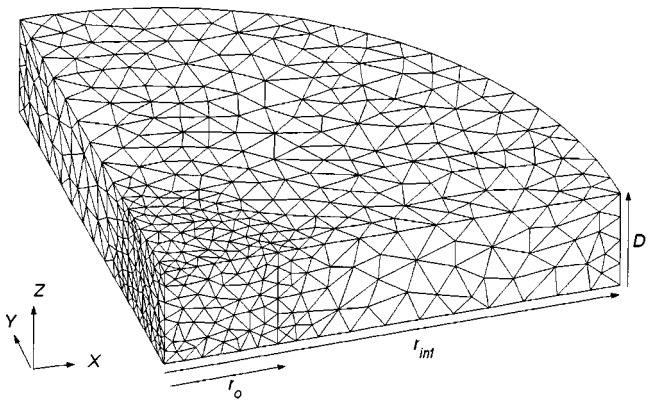

Fig. 1. FEM of cartilage specimen.

IV. Materials and Methods

A. Tissue Preparation

Fresh cartilage specimens from domestic pigs were obtained from a local packing house (Farmers John, Vernon, CA) and harvested as described by Wong *et al.* [10]. Several cartilage grafts from each septal cartilage were obtained and sectioned into rectangular slabs measuring 25 mm × 30 mm with thickness of 1–4 mm. Uniform specimen thickness was accomplished by removing the outermost layers of the intact full-thickness septal cartilage using a commercial rotary food slicer (model 620, Chef's Choice Int., EdgeCraft Corp, Avondale, PA) until the desired thickness was reached [11]. Specimens were then kept in saline solution until testing.

B. Temperature Measurement

PNC specimens were irradiated during 1–15 s using Nd : YAG laser ($\lambda = 1.32$ μm, 50-Hz PRR, Laser Aesthetics, Auburn, CA) using several laser powers (1–10 W). Laser energy was delivered using a 400-μm core-diameter silica multimode optical fiber terminating in a collimating lens. Laser spot size (2.5-mm radius) and power were measured with thermal paper and a pyroelectric meter (Model 200/10, Coherent, Auburn, CA), respectively.

Surface temperature (T_s) was measured using an infrared emission sensor [response time of 120 ms (95%), spectral sensitivity 7.6–18 μm, Laser Aesthetics] and calibrated using a hot/cold blackbody calibration source (Model BB701, Omega Engineering Inc., Stamford, CT) set at different known temperatures. A Teflon-insulated type E thermocouple (Chromega-Constantan 0.005-in wire diameter 5TC-TT-E-36-36 with cold

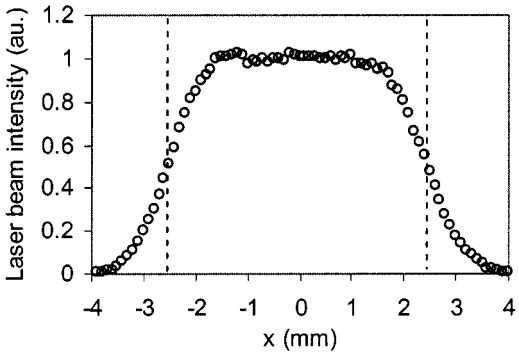

Fig. 2. Spatial distribution of the laser-beam intensity. Dashed lines indicate locations where intensity decays to 50% of its maximum value.

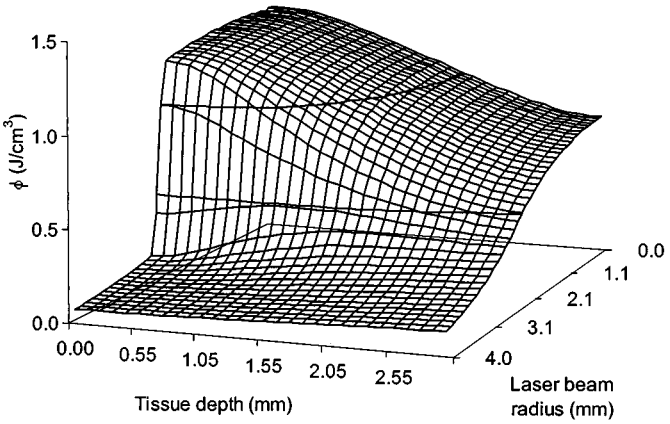

Fig. 3. Fluence rate distribution versus tissue depth and laser-beam radius in a 3-mm-thick slab of cartilage relative to a radiant exposure of 1 J/cm^2.

junction compensator, M60/1290, MCJ Series, Omega Engineering Inc.) was used to measure temperature inside the cartilage specimen $(T_{\rm cart})$ at a depth halfway through the specimen thickness. The sensor signal was amplified and low-pass filtered (3-dB cutoff at 30 Hz) with a low-noise preamplifier (model SRS 560, Stanford Research Systems, Sunnyvale, CA). An analog-to-digital converter (AT-MIO-16XE-50, National Instruments, Austin, TX) was used to record T_s and $T_{\rm cart}$ using software written in LabVIEW (National Instruments) running on a personal computer (AMD, 750 MHz).

C. Laser-Beam Profile Measurement

The laser-beam intensity profile was measured by repeatedly irradiating the tip of a thermocouple at different locations across the beam diameter. At each location x, the maximum temperature change $\Delta T_{\max}(x)$ experienced by the sensor was assumed to be proportional to the spatial distribution of the beam intensity, since parameters such power (5 W) and irradiation time (1 s) were kept constant throughout the experiment. The thermocouple was mounted on a three-axis micropositioner with the sensor tip located 40-mm away from the laser lens, the distance at which the cartilage surface is normally kept from the light source during irradiation. To avoid uneven heating of the sensor, only the tip of the thermocouple was directly exposed to the laser beam, keeping the leads of the thermocouple insulated and parallel to the beam.

The profile was then obtained from the $\Delta T_{\max}(x)$ plot, as shown in Fig. 2. The temperature change measured at each location was normalized with respect to the average temperature change recorded at points near the approximate center of the laser beam ($-1 < x < 1$ mm). The beam radius was defined as the location x where the laser-beam intensity decays to 50% of its maximum value, indicated by dashed lines in Fig. 2. The resultant beam radius $r = 2.5$ mm agreed well with the direct measurement of beam radius obtained using thermal paper.

The thermocouple response to different laser-beam powers P (W) was evaluated showing a linear relationship between $\Delta T_{\max}$ and P. This result further supports the postulate that the temperature change experienced by the sensor is proportional only to the spatial distribution of the laser-beam intensity.

D. Estimation of Fluence Rate in Cartilage

Laser irradiation of tissue transforms into thermal energy deposition. Efficacy of this transformation depends on the laser wavelength and optical properties of the tissue involved. Optical properties of PNC at a wavelength of 1.32 μm are characterized by low absorption $\mu_a = 100$ m^{-1}, high scattering $\mu_s' = \mu_s(1-g) = 260$ m^{-1}, and mean cosine of the scattering angle $g \approx 0.9$ [12]. Tissue index of refraction n was assumed to be 1.37. Fig. 3 illustrates the fluence rate distribution in a 3-mm-thick cartilage specimen as a function of tissue depth and radius, obtained from the Monte Carlo simulation. A flat laser-beam profile of 2.5 mm in radius and a unitary irradiance of 1 J/cm^2 were used as input parameters to the multilayer Monte Carlo (MLMC) and convolution (CONV) codes [7], [8].

Since MLMC/CONV algorithms and FEMLAB are independent software, the calculated fluence rate distribution $\phi(r,z)$, was incorporated into FEMLAB as a combination of radial (r) and axial (z) dependent functions. The first expression is a modified error function in terms of the radius (in nm)

$$\phi(r) = (1/2)\mathrm{erfc}\,[4(r - r_0)] \tag{7}$$

where r_o is the radius of the source. The second expression is a gaussian fit for the fluence rate attenuation along the tissue depth at the beam center $(r = 0)$, given as

$$\phi(z) = Y_o + \frac{A}{w\sqrt{\pi/2}} \exp -2\frac{(z - z_o)^2}{w^2} \tag{8}$$

where Y_o, A, w, and z_o are fitting coefficients. Using (7) and (8), $\phi(r,z)$ can be incorporated in the analysis as a product of two functions $\phi(r,z) = \phi(r) \cdot \phi(z)$ as plotted in Fig. 4.

In addition to wavelength and optical properties, $\phi(x,y,z)$ depends on the laser-beam characteristics and thickness D of the irradiated specimen. In our calculations, only the latter changed since the tissue optical properties were considered constant in the temperature range of interest (20 °C–100 °C) and the laser-beam profile was measured and remained unchanged. Fig. 5 shows curves of $\phi(z)$ as a function of tissue depth, calculated at the center of the laser beam for three different thicknesses of cartilage.

The curves shown in Fig. 5 were obtained from the Monte Carlo simulation. A set of curve fitting coefficients Y_o, A, w,

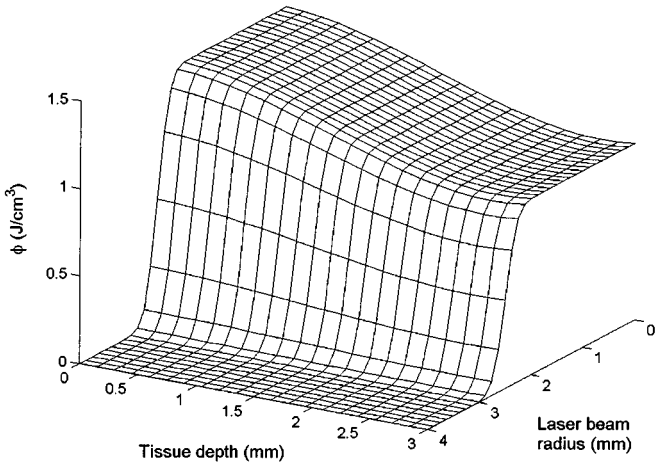

Fig. 4. Fluence rate distribution versus tissue depth and laser-beam radius in a 3-mm-thick slab of cartilage obtained using (7) and (8).

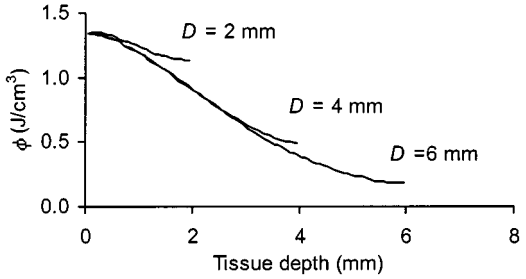

Fig. 5. Predicted $\phi(z)$ as a function of tissue depth at the center of the laser beam. Calculations for specimen thickness of 2, 4, and 6 mm.

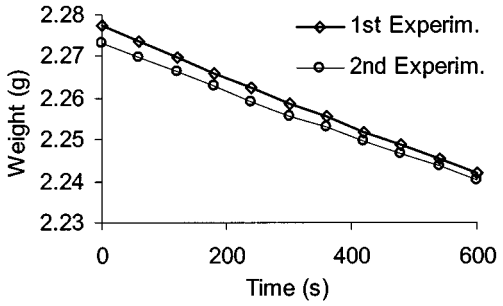

Fig. 6. Mass-transfer rate of water in cartilage due to evaporation.

and z_o, as defined in (8) were calculated for each curve. In this fashion, a database of curve fitting coefficients for different thicknesses was created and incorporated into the finite-element code.

E. Mass–Transfer Rate Measurement

A first estimation of the mass-transfer coefficient h_m involved in the evaporative cooling was indirectly obtained by measuring the mass-transfer rate n_{vap} of water in cartilage to the atmosphere. A rectangular slab of cartilage (52 × 18 × 2 mm) was left to dry at room temperature for 10 min on top of a microbalance (Model R200D, SY Nielson Service Inc., Riverside, CA). The mass-transfer rate was estimated from the slope of the weight vs. time plot, shown in Fig. 6. The experiment was repeated a second time following a period (10 min) of specimen rehydration in saline solution. From this graph, n_{vap} is found to be ≈7E-8 (kg/s).

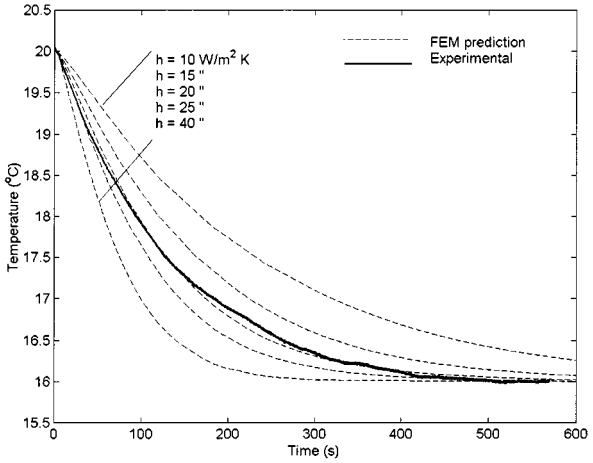

Fig. 7. Experimental and FEM predictions of the temperature history in a specimen of cartilage during evaporation.

A second experiment was designed to measure the transient and steady-state temperatures of cartilage during the evaporative cooling process. Using a needle, a thermocouple was inserted in to the center of a square slab of cartilage (15 × 15 × 3 mm). The specimen was initially kept in saline solution at 20 °C. Subsequently, the specimen was taken out of the solution, excess superficial water was removed, and dried at room temperature until thermal equilibrium was reached.

Fig. 7 illustrates the temperature–time plot, showing a steady-state temperature of the cartilage specimen, $T_{\text{cart}} \cong 16$ °C at time $t > 500$ s. This equilibrium temperature is in fact equivalent to the so-called wet bulb temperature, which can be obtained from a psychrometric chart with known room temperature ($T_\infty = 23$ °C) and relative humidity ($Rh = 50\%$). Finally, using (5), the mass-transfer coefficient h_m was found to be ≈20E-3 (m/s).

F. Estimation of Convective Heat and Mass-Transfer Coefficients

The temperature-time history shown in Fig. 7 (evaporative cooling effect) was used to estimate both heat and mass-transfer coefficients. In the absence of irradiation, conservation of energy in a cartilage specimen in air reduces to a balance between latent energy lost by liquid evaporation and energy transfer to the liquid from the surrounding environment, which may be expressed as

$$h(T_\infty - T_s) = h_{fg} h_m \left[\rho_{\text{vap, sat}}(T_s) - \rho_{\text{vap},\infty}\right]. \quad (9)$$

After thermal equilibrium is attained ($t > 500$ s), enough information is known ($T_\infty = 23$ °C, $T_s = 16$ °C, $Rh = 50\%$) to determine a ratio between the heat and mass-transfer coefficients, given as

$$\frac{h}{h_m} = \frac{h_{fg}\left[\rho_{\text{vap, sat}}(T_s) - \rho_{\text{vap},\infty}\right]}{(T_\infty - T_s)}. \quad (10)$$

Equation (10) can then be substituted into (1) with $Q_i = 0$ and solved numerically using the FEM. Fig. 7 shows a single

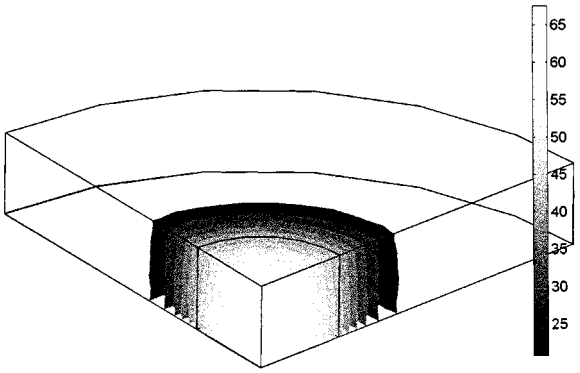

Fig. 8. FEM prediction of the temperature distribution in a 2.3-mm-thick cartilage at the end of laser irradiation ($t = 10$ s, $P = 5$ W).

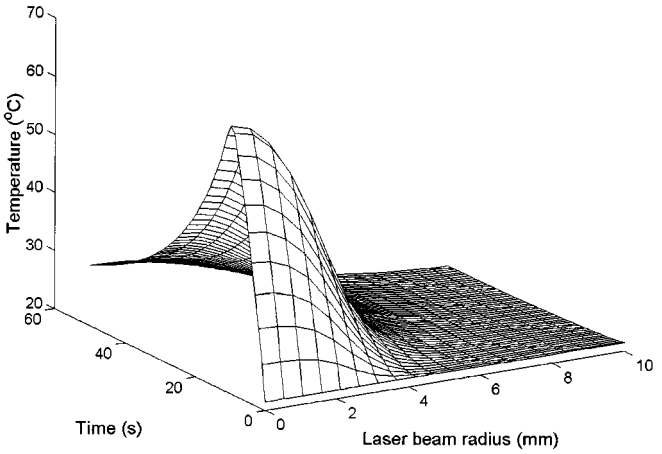

Fig. 9. Surface temperature history of a 2.3-mm-thick cartilage during and after laser irradiation ($t = 10$ s, $P = 5$ W).

experimental temperature–time curve along with several curves obtained using the FEM for different values of h.

The FEM predictions of temperature during water evaporation agreed very well with the experimental result when values for h of 15–20 W/m^2·K were used as input parameters in the computer simulation. This range is in close agreement with typical values of h for free convection in gases, which range between 5–25 W/m^2·K [9]. Substituting h in (10) gives values for the mass-transfer coefficient h_m between 13E-3 and 17E-3 (m/s), which are in good agreement with those obtained previously (Section IV-E).

V. Results

A. Thermal Response of Cartilage—Model Predictions

Fig. 8 shows the tissue response to laser irradiation as predicted by the FEM. The figure presents several isothermal surfaces showing the temperature distribution in a 2.3-mm-thick PNC specimen at the end of irradiation ($t = 10$ s, $P = 5$ W). As expected, the FEM predicts higher temperatures at the center of the beam and at regions nearest to the irradiated surface (bottom surface in the model).

Fig. 9 presents the surface temperature history along the radius of the model ($0 < r < 10$ mm) for the same specimen.

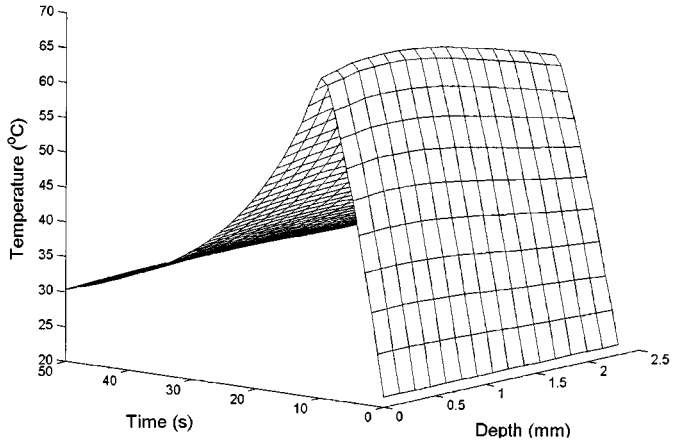

Fig. 10. Temperature variation as a function of tissue depth at the center of the laser target site. Prediction made for a 2.3-mm-thick cartilage during and after laser irradiation ($t = 10$ s, $P = 5$ W).

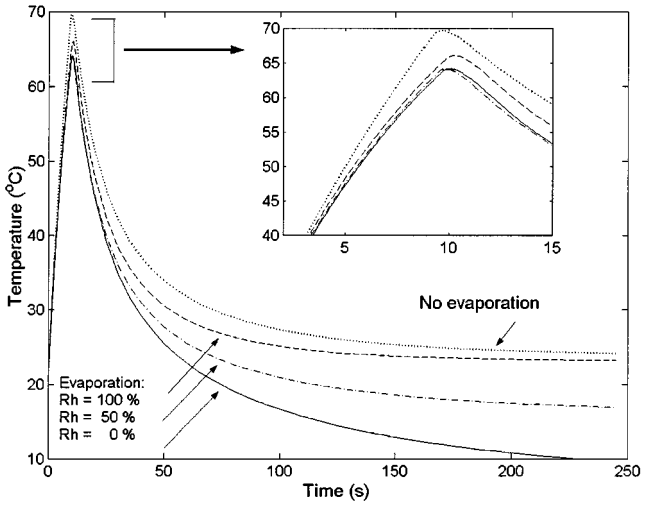

Fig. 11. Surface temperature history of a 2.3-mm-thick cartilage during and after laser irradiation ($t = 10$ s, $P = 5$ W). Comparison between calculations made for different environmental conditions.

It is clear that heating is a highly localized phenomenon almost limited to the laser target site, where significant temperature gradients develop. The temperature rapidly increases to a value of 60 °C; thermal relaxation follows after irradiation until thermal equilibrium with the environment is reached.

Fig. 10 illustrates temperature variation as a function of tissue depth, measured at the center of the laser irradiation site ($r = 0$). The calculation shown corresponds to a 2.3-mm-thick specimen; at this tissue thickness, the difference in temperature between front ($z = 0$ mm) and back ($z = 2.3$ mm) surfaces after laser irradiation ($t = 10$ s) is about 5 °C. This difference becomes significant as thickness increases. For instance, if the specimen were 1-mm thicker ($D = 3.3$ mm), the difference would be close to 15 °C. The maximum temperature occurs inside the tissue ($z \cong 0.5$ mm) near the irradiated surface. This maximum temperature is about 2 ° higher than that of the front surface.

Fig. 11 illustrates the temperature history of a point located at the surface and center of the laser beam ($z = 0$, $r = 0$) when the cooling effect of evaporation is incorporated in to the

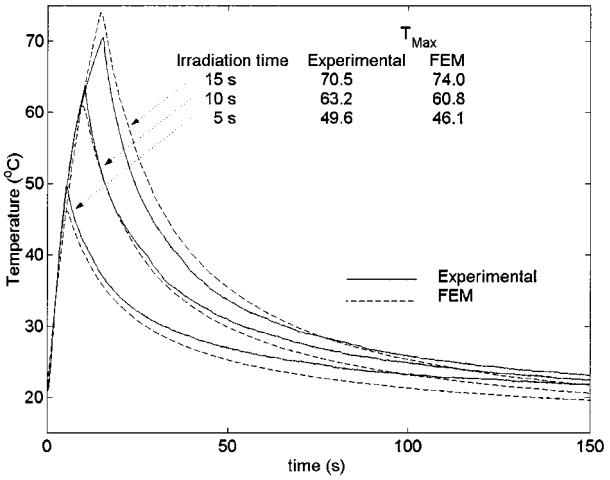

Fig. 12. Surface temperature history of a 2.3-mm-thick cartilage during and after laser irradiation ($P = 5$ W). Comparison between experimental and FEM predictions for different irradiation times.

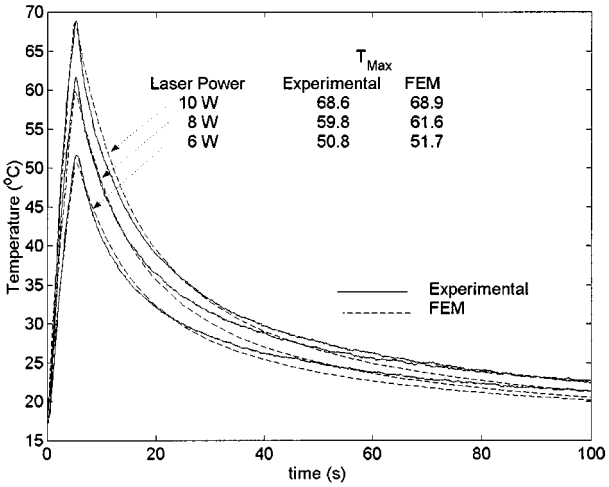

Fig. 13. Surface temperature history of a 3.3-mm-thick cartilage during and after laser irradiation ($t = 5$ s). Comparison between experimental and FEM predictions for different laser powers (6–10 W).

model. Values of Rh varying from dry (0%, maximum evaporation) to saturated air (100%, minimum evaporation) were used in the calculations. Fig. 11 also shows the temperature history as predicted by the model without water evaporation. Comparison among the curves reveals the importance of including water evaporation in the calculation of temperature. It can be seen that evaporation influences mainly the final temperature of the tissue; however, evaporation also affects the heating rate and therefore the maximum temperature reached after laser irradiation, as shown in the amplified view of the peak temperature in Fig. 11.

B. Measurements and Model Predictions

In Fig. 12, the surface temperatures predicted by the FEM are compared with temperatures measured experimentally during laser irradiation of a 2.3-mm-thick cartilage specimen. The laser power was set at 5 W while the irradiation time varied from 5 to 15 s. After each exposure, the specimen was immersed in saline solution for 10 min for rehydration. In this comparison, the FEM predicted temperatures correspond to the average surface temperatures of the region within a radius of 2 mm from the center of the irradiation site. The reason for doing this arithmetic mean is that the experimental measurement made with the infrared device is the average temperature of the entire surface within the field of view of the instrument, which is close to the detector aperture ($r = 2.5$ mm) at a sensor to object distance of 30 mm. Fig. 12 shows good agreement between numerical and experimental results. The FEM predicts maximum temperatures at the end of the irradiation period well within a 10% error with respect to the experimental values. During thermal relaxation, the predicted curves deviate from the experimental results by showing higher cooling rates. This discrepancy might be due to localized cartilage dehydration after irradiation at regions near the beam spot. Theses reductions in water concentration results in lower water loss rates, which in turn affect the evaporative cooling effect.

In Fig. 13, experimental and predicted surface temperatures of a 3.3-mm-thick cartilage specimen are compared. In this case, the laser irradiation time was fixed at 5 s while varying the laser-beam power from 6 to 10 W. As described above, the specimen was allowed to rehydrate after each exposure. The surface temperatures predicted by the FEM show excellent agreement (within 5%) with experimental measurements. Fig. 14 also compares predicted and measured temperatures, but for a 0.95-mm-thick cartilage specimen. Here as well, the laser irradiation time was fixed at 5 s and the laser-beam powers used were 4–8 W. In contrast to the results shown in Fig. 13, the FEM predictions for the 0.95-mm-thick specimen overestimate (>10%) the experimental temperature at the end of the irradiation when the laser parameters used led to surface temperatures above 50 °C.

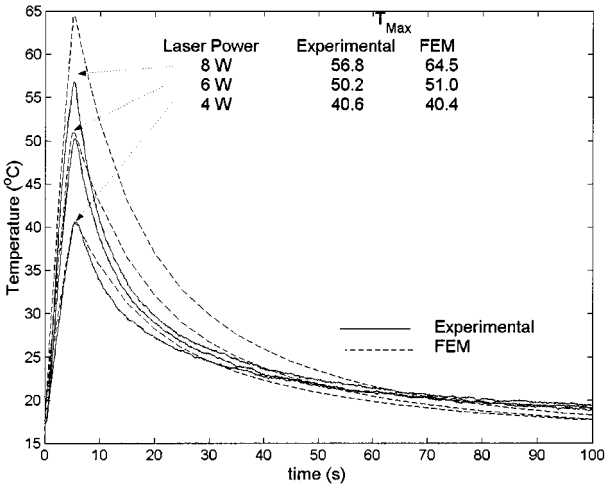

Fig. 14. Fluence rate distribution versus tissue depth and laser-beam radius in a 3-mm-thick slab of cartilage obtained using (7) and (8).

The discrepancies between measured and predicted results illustrated in Fig. 14 may be explained in terms of the tissue water concentration. A thin specimen should dehydrate faster than a thick one under the same conditions, since the water volume per unit area in the former is lower. If we now postulate that light absorption (thermal energy deposition) depends on water concentration, then results from our FEM are more likely to deviate from experiments made on thinner specimens, since the model

assumes constant water transfer rates from the tissue to the surroundings. Furthermore, water concentration in cartilage may influence both, convective heat and mass-transfer coefficients, making both time and temperature dependent. However, our calculations assume these coefficients constant.

VI. Discussion

In this study, we performed the experimental characterization of the thermal response of PNC that accompanies Nd:YAG ($\lambda = 1.32$ μm) laser irradiation. The surface temperature history was monitored during heating and thermal relaxation; using laser exposure times ranging between 1 and 15 s and laser powers of 1–10 W, which are parameters typically used for cartilage reshaping. The experimental results were then used to validate a FEM of the temperature response of laser-irradiated tissue. The numerical model accounts for heat diffusion, light propagation in tissue and heat loss due to water evaporation. Due to its optical properties, photothermal heating of cartilage is a scattering dominated phenomenon. Hence, the photon density distribution in cartilage was estimated using a numerical solution of light propagation that included scattering. In addition to light interactions, the cooling effect of water evaporation at the tissue–air interface proved to have an important influence on the thermal response of cartilage. The experimental observations are supported by numerical results when vaporization is included in calculations of temperature. From the experimental results, heat and mass-transfer coefficients were measured and found to be within the range of typical values for convective heat transfer in gases.

The good agreement observed between FEM and experimental results are indicative that the major contributors determining the thermal response of cartilage to laser irradiation have been taken into account. Nevertheless, we are aware of the limitations of our approach, since several physical processes have been excluded from the FEM analysis. For instance, our model does not incorporate heat loss due to the low-energy phase transformations, which are known to take place in cartilage above a critical temperature $T_c \cong 65$ °C [3]. It is also known that the changing tissue optical properties alter the rate of energy deposition in tissue, thereby accelerating optical changes in some parts of the tissue [13]. Furthermore, temperature gradients in cartilage induce water transport across the tissue from irradiated to nonirradiated zones, which may in turn have a significant effect on the heat and mass-transfer and light absorption coefficients. Therefore, a complete formulation of the thermal response of cartilage to laser heating should incorporate water mass transfer in bulk cartilage, which might in turn influence laser energy deposition rates and surface evaporation kinetics. We are currently addressing several of these issues.

VII. Summary

Laser irradiation can be used to reshape cartilage into complex geometries and has the potential to alter the practice of head and neck reconstructive surgery. However, due to the few practical clinical laser applications on cartilage and no procedures that use low-intensity nonablative fluence with the exception of laser reshaping, the thermal and optical behavior of cartilage has been largely uninvestigated.

The experimental work has led to the formulation and validation of the numerical model. The information rendered by the FEM will in turn, allow us to make predictions of: 1) the onset of new molecular arrangements in the material (phase change), which hypothetically are responsible of permanent shape change, and 2) estimation of thermal damage (denaturation) from the spatial and temporal temperature distribution using the so-called Arrhenius integral formulation (Pearce and Thomsen, 1995). By determining the thresholds and limits of both rate processes, a comprehensive relationship among the treatment parameters involved (time, tissue thickness, irradiance, etc.) will be established, thus, conceiving the fundamental guidelines of LARC.

Acknowledgment

The authors would like to thank J. S. Nelson and S. Tanenbaum for valuable discussions.

References

[1] B. J. F. Wong, T.E. Milner, B. Anvari, A. Sviridov, A. Omel'chenko, V. V. Bagratashvili, E. N. Sobol, and J. S. Nelson, "Measurement of radiometric surface temperature and integrated back-scattered light intensity during feedback controlled laser-assisted cartilage reshaping," *Lasers Med. Sci.*, vol. 13, no. 1, pp. 66–72, 1998.

[2] Z. Wang, M. M. Pankratov, D. F. Perrault, and S. M. Shapshay, "Laser-assisted cartilage reshaping: *In vitro* and *in vivo* animal studies," *Proc. SPIE*, vol. 2395, pp. 296–302, 1995.

[3] E. N. Sobol, A. Sviridov, V. V. Bagratashvili, A. Omel'chenko, Y. M. Ovchinnikov, A. B. Shekhter, V. M. Svistishkin, and A. N. Shinaev, "Laser reshaping of nasal septum cartilage: Clinical results for 40 patients," *Proc. SPIE*, vol. 3907, pp. 297–302, May 2000.

[4] E. N. Sobol, *Phase Transformations and Ablation in Laser-Treated Solids*. New York: Wiley, 1995, pp. 316–322.

[5] J. Pearce and S. Thomsen, "Rate process analysis of thermal damage," in *Optical–Thermal Response of Laser-Irradiated Tissue*, A. J. Welsh and M. J. C van Gemert, Eds. New York: Plenum, 1995, pp. 561–606.

[6] C. S. Orr and R. C. Eberhart, "Overview of bioheat transfer," in *Optical–Thermal Response of Laser-Irradiated Tissue*, A. J. Welsh and M. J. C. van Gemert, Eds. New York: Plenum, 1995, pp. 367–384.

[7] L. H. Wang, S. L. Jacques, and L. Q. Zheng, "MCML—Monte Carlo modeling of photon transport in multi-layered tissues," *Comput. Methods Programs Biomed.*, vol. 47, no. 2, pp. 131–146, July 1995.

[8] ——, "CONV—Convolution for responses to a finite diameter photon beam incident on multi-layered tissues," *Comput. Methods Programs Biomed.*, vol. 54, no. 3, pp. 141–150, Nov. 1997.

[9] F. P. Incropera and D. P. DeWitt, *Fundamentals of Heat and Mass Tranfer*. New York: Wiley, 1996.

[10] B. J. F. Wong, K. K. H. Chao, H. K Kim, E. A. Chu, X. Dao, M. Gaon, C. H. Sun, and J. S. Nelson, "The porcine and lagomorph septal cartilages: Models for tissue engineering and morphologic cartilage research," *Amer. J. Rhinology*, vol. 15, no. 2, pp. 109–116, Mar.-Apr. 2000.

[11] S. Diaz, E. Lavernia, and B. J. F. Wong, "Mechanical behavior of cartilage during laser irradiation," *Proc. SPIE*, vol. 4257, pp. 192–197, 2001.

[12] J. I. Youn, S.A. Telenkov, E. Kim, N. C. Bahavaraju, B. J. F. Wong, J. W. Valvano, and T. E. Milner, "Optical and thermal properties of nasal septal cartilage," *Lasers Surgery Med.*, vol. 27, no. 2, pp. 119–128, Aug. 2000.

[13] S. L. Jacques, "Role of tissue optics and pulse duration on tissue effects during high-power laser irradiation," *Appl. Opt.*, vol. 32, no. 13, pp. 2447–2454, May 1993.

Sergio H. Díaz received the B.S. degree in mechanical engineering from the National Autonomous University of Mexico, Mexico City, Mexico, in 1993, the M.S. degree in mechanical engineering from McGill University, Montreal, QC, Canada, in 1995, and the Ph.D. degree in mechanical engineering from Imperial College, London, U.K., in 2000.

He became a Post-Doctoral Researcher with the Beckman Laser Institute at the University of California, Irvine, in September 2000. His current research interests include smart materials and composite structures, finite-element methods, nondestructive evaluation, and laser irradiation for reconstructive surgery, particularly cartilage reshaping.

Guillermo Aguilar received the B.S. degree in mechanical engineering from the National Autonomous University of Mexico, Mexico City, Mexico, in 1993, and the M.S. and Ph.D. degrees in mechanical engineering from the University of California, Santa Barbara, in 1995 and 1999, respectively.

He became a Post-Doctoral Researcher with the Beckman Laser Institute and the Department of Chemical and Biochemical Engineering and Material Science at the University of California, Irvine, (UCI) in 1999. He is currently an Adjunct Assistant Professor with the Center for Biomedical Engineering, UCI. His current research interests include cryogen spray atomization and heat transfer, application of cryogen sprays and laser irradiation in dermatology, and therapeutic applications of lasers in dermatology and reconstructive surgery.

Enrique J. Lavernia received the B.S. degree in solid mechanics from Brown University, Providence, RI, in 1982 and the M.S. degree in metallurgy and the Ph.D. degree in materials engineering from the Massachusetts Institute of Technology, Cambridge, in 1984 and 1986, respectively.

Since 1998, he has been a Professor and Chair of the Department of Chemical Engineering and Material Science, University of California, Irvine. He also holds joint appointments with the Department of Mechanical and Aerospace Engineering and the Center for Biomedical Engineering. His current research interests include the processing of structural materials and metal matrix composites, with particular emphasis on solidification fundamentals, rapid solidification processing, spray atomization and deposition of structural materials, solidification processing of metal matrix composites, and mathematical modeling of advanced materials and processes.

Brian J. F. Wong was born in Southern California. He received the B.S. degree (*summa cum laude*) in biomedical engineering from the University of Southern California, Los Angeles, the M.D. degree from the Johns Hopkins University, Baltimore, MD, in 1990, and the Ph.D. degree in photo medicine from the University of Amsterdam, Amsterdam, The Netherlands, in 2001.

He also studied engineering at Oxford University as a Rotary Foundation Scholar. He completed fellowship training in facial plastic surgery at University of California, Irvine, and is board certified in Head and Neck Surgery—Otolaryngology. He is an Associate Professor in the Division of Facial Plastic Surgery in the Otolaryngology Department and has joint appointments in the Whitaker Center for Biomedical Engineering and the Beckman Laser Institute at University of California, Irvine. He has authored or coauthored over 50 papers. His current research interests are in the field of biomedical engineering with specific interests in medical device development and laser applications in medicine.

Dr. Wong is a Fellow of the American College of Surgeons. He received the National Institutes of Health Clinical Investigator Development Award.